Dewan Riset & Pengabdian kepada Masyarakat

Energy Technology - Ersan

Molecular-Glass Interface Engineering Enables Highly Efficient and Stable Inverted Perovskite Solar Cells

Document Details

Submission ID
trn:oid:::3618:147671251

Submission Date
Aug 8, 2026, 12:13 PM GMT+7

Download Date
Aug 8, 2026, 12:38 PM GMT+7

File Name
Energy Technology - Ersan.docx

File Size
7.2 MB

25 Pages

6,899 Words

42,518 Characters

16% Overall Similarity

The combined total of all matches, including overlapping sources, for each database.

Filtered from the Report

- Bibliography
- Quoted Text

Match Groups

18 Not Cited or Quoted 14%
Matches with neither in-text citation nor quotation marks

2 Missing Quotations 1%
Matches that are still very similar to source material

0 Missing Citation 0%
Matches that have quotation marks, but no in-text citation

0 Cited and Quoted 0%
Matches with in-text citation present, but no quotation marks

Top Sources

8% Internet sources
12% Publications
10% Submitted works (Student Papers)

Integrity Flags

0 Integrity Flags for Review

Our system's algorithms look deeply at a document for any inconsistencies that would set it apart from a normal submission. If we notice something strange, we flag it for you to review.

A Flag is not necessarily an indicator of a problem. However, we'd recommend you focus your attention there for further review.

Match Groups

- **18** Not Cited or Quoted 14%
  Matches with neither in-text citation nor quotation marks
- **2** Missing Quotations 1%
  Matches that are still very similar to source material
- **0** Missing Citation 0%
  Matches that have quotation marks, but no in-text citation
- **0** Cited and Quoted 0%
  Matches with in-text citation present, but no quotation marks

Top Sources

8% Internet sources
12% Publications
10% Submitted works (Student Papers)

Top Sources

The sources with the highest number of matches within the submission. Overlapping sources will not be displayed.

1	Internet	pubs.rsc.org 2%
2	Internet	www.tdx.cat 1%
3	Publication	Kai-Kai Liu, Ze-Fan Yao, Deng Wang, Xiaofeng Huang et al. "Polymerized Y-series ... <1%
4	Student papers	University of Sheffield on 2016-05-03 <1%
5	Internet	dspace.vutbr.cz <1%
6	Publication	Jingyang Liao, Xiying Zhang, Shuaishuai Guo, Shaohua Zhang, Xiaotian Hu, Yiwan... <1%
7	Publication	Md. Anwer Hossain, Md Rasidul Islam, Naseem Akhter, Sobhi M. Gomha, Magdi E.... <1%
8	Internet	journal.hep.com.cn <1%
9	Internet	qspace.library.queensu.ca <1%
10	Publication	Ersan Y. Muslih, Neng Hani Handayani, Masahiro Nakano, Makoto Karakawa et al... <1%

11 Student papers
Indian Institute of Technology Bhilai on 2024-05-29 <1%

12 Publication
Tazkiaturrizki Tazkiaturrizki, Sandyanto Adityosulindro, Djoko Mulyo Hartono, Se... <1%

13 Student papers
Mahidol University on 2026-01-02 <1%

14 Student papers
University of the Western Cape on 2021-05-18 <1%

15 Publication
Zhijie Wang, Cheng Gong, Cong Zhang, Chenxu Zhao, Tzu-Sen Su, Haiyun Li, Hong... <1%

16 Internet
link.springer.com <1%

17 Student papers
Anna University on 2026-03-10 <1%

18 Publication
Chang, Chih-Yu, Kuan-Ting Lee, Wen-Kuan Huang, Hao-Yi Siao, and Yu-Chia Chang... <1%

19 Publication
Xiaomei Lian, Jiehuan Chen, Shiqi Shan, Gang Wu, Hongzheng Chen. " Polymer M... <1%

20 Internet
os.unil.cloud.switch.ch <1%

Molecular-Glass Interface Engineering Enables Highly Efficient and Stable Inverted Perovskite Solar Cells

Ersan Y. Muslih[1,2], Neng Hani Handayani[3], Masahiro Nakano[4], Makoto Karakawa[3,4,5], Mohammad Ismail Hossain[6], Md. Akhtaruzzaman[7], Jean-Michel Nunzi[5,8*], Olivier Lebel[9*] Tetsuya Taima[3,4,5*], and Md. Shahiduzzaman[4,5*]*

[1]Environmental Engineering Department, Faculty of Architecture Landscape and Environmental Engineering, Universitas Trisakti, Jakarta 11440, Indonesia

[2]Center of Excellent for Sustainable Energy and Materials, Universitas Trisakti, Jakarta 11440, Indonesia

[3]Graduate School of Frontier Science Initiative, Kanazawa University, Kakuma, Kanazawa 920-1192, Japan

[4]Graduate School of Natural Science and Technology, Kanazawa University, Kakuma, Kanazawa 920-1192, Japan

[5]Nanomaterials Research Institute, Kanazawa University, Kakuma, Kanazawa 920-1192, Japan

[6]Department of Electrical and Computer Engineering, University of California, Davis, CA 95616, USA

[7]Department of Chemical Engineering, Faculty of Engineering, Islamic University of Madinah, Madinah 42351, Saudi Arabia

[8]Department of Physics, Engineering Physics and Astronomy, Queens University, Kingston, Ontario K7L 3N6, Canada

[9]Department of Chemistry and Chemical Engineering, Royal Military College of Canada, Kingston, K7K 7B4, ON, Canada

*Corresponding authors

Abstract

Perovskite solar cells (PSCs) with inverted configuration (p-i-n) offer simple, low-temperature fabrication and high open-circuit voltage (V_{OC}), but they are limited by poor thermal and moisture stability. Here, we introduce solution-processable amorphous molecular glass electron-acceptor interlayers, comprising two fused fluoranthene imide (FFI) derivatives and a diketopyrrolopyrrole (DPP) analogue, which simultaneously enhance the efficiency and operational durability of $MAPbI_3$ p-i-n devices. These glassy films utilize strong π–π stacking, electron-withdrawing triazine and thiophene units, and inherent hydrophobicity to optimize energy-level alignment with PCBM, reduce ion migration, and prevent moisture ingress. The addition of FFI increases the champion power conversion efficiency (PCE) from 14.6% to 15.5% and raises the water contact angle from 77° to 108°. Under continuous maximum power point (MPP) tracking at 85 °C, FFI-modified cells retain over 90% of their initial PCE after 96 hours, while control devices degrade within 48 hours. X-ray diffraction and UV–Vis measurements confirm the sustained integrity of the α-phase and minimal formation of PbI_2. This interfacial engineering approach offers a scalable pathway to high-performance, durable perovskite photovoltaics.

Keywords: Inverted (p-i-n) Perovskite solar cells, Molecular glass interlayers, Energy-level alignment, Ion-migration suppression, Operational Stability

1. Introduction

Perovskite solar cells (PSCs) have emerged as one of the most promising photovoltaic technologies due to their high-power conversion efficiency (PCE) exceeding 26% for n-i-p and p-i-n structure [1–6] yet with a low fabrication cost. However, their commercialization is hindered by stability issues and the need for efficient electron transport layers (ETLs) to optimize charge extraction. Traditional ETLs for n-i-p structures, like TiO2, have inherent limitations such as poor stability, low conductivity, and complex processing conditions. They are not suitable for p-i-n structures because they require higher annealing temperatures than the perovskite itself [7–11]. Thus, in p-i-n structure, ETLs such as phenyl-C_{61}-butyric acid methyl ester (PCBM) is a common material due to low application temperature. In addition, PCBM molecules, whether blended into the bulk or added as a single layer as ETLs in devices, enhance electron transfer and can effectively reduce hysteresis [12–18]. However, the PCBM still has some shortcomings, such as it can still react with methylammonium iodide (MAI) or iodine ions, cannot repel H_2O molecules from outside, and even PCBM can penetrate into the perovskite grain boundaries,

resulting in damage to the perovskite and a decrease in device performance [19–23]. Thus, interfacial modification with interlayer material helps protect the perovskite layer from ion migration and moisture-induced degradation, thereby improving long-term stability.

Interface modification has long been explored as a key strategy to improve both the efficiency and stability of perovskite solar cells. Among the reported approaches, ethylenediamine (EDA) has been used in Sn–Pb perovskites, where it successfully reduces trap states and enhances charge extraction[24]. However, despite these advantages, EDA suffers from several drawbacks: its volatile and corrosive nature, combined with limited long-term stability, significantly restricts its practical application. By contrast, the molecular glass electron-acceptor compounds introduced in this work provide a distinct and advantageous alternative. Unlike EDA, these materials are structurally robust, non-volatile, and capable of forming amorphous glassy interlayers that intimately coat the perovskite surface. Furthermore, they integrate defect passivation with additional functionalities, including hydrophobic protection, suppression of ion migration, and improved compatibility with PCBM. As a result, the molecular glass electron-acceptor compounds represent an evolutionary step in interfacial engineering, merging the defect passivation of earlier strategies, the multifunctionality of bifunctional ligands, and the robustness of glass-forming molecular systems. Collectively, these unique features establish them as a promising route toward achieving high-performance and durable perovskite solar cells.

In this study, we present molecular glass electron-acceptor derivatives as potential interlayer materials between perovskite and PCBM in a p-i-n structure, and thoroughly examine their influence on device performance. These molecular glass derivatives are especially appealing due to their strong π-bonding, extended delocalization, and inherent hydrophobic properties. Additionally, they showcase excellent electron mobility, high photostability, and significant chemical tunability, making them versatile for interfacial engineering [25–34]. Beyond these inherent benefits, this research also investigates how the distinct electronic and chemical interactions of the molecular glass interlayers prevent the degradation of methylammonium lead iodide ($MAPbI_3$) into lead iodide (PbI_2). Consequently, adding these materials not only boosts the efficiency of perovskite solar cells but also greatly enhances their operational stability.

2. Experimental

2.1. Materials

The fluorine-doped tin oxide (FTO) glass, with a thickness of 0.7 mm, resistivity of 9-10 Ω per square, and transmittance of 82-85%, was obtained from Nippon Sheet Glass Co., Ltd. (Tokyo, Japan). Acetone (C_3H_6O, 99.5% purity) and isopropanol (IPA, C_3H_8O, 99.5% purity) were sourced from Tokyo Chemical Industry Co., Ltd. (Tokyo, Japan). Lead iodide (PbI_2, 99.9% purity) was acquired from Tokyo Chemical Industry (Tokyo, Japan). N,N-dimethylformamide (DMF, 99.5% purity) were supplied by Wako Chemical (Tokyo, Japan). Dimethyl sulfoxide (DMSO, 99.5% purity), nickel nitrate pentahydrate ($Ni(NO_3)_2.5H_2O$, 99.9 % purity), methylammonium iodide (MAI, anhydrous, >99.9% purity), and ethanol (C_2H_6O, >99.9% purity) were obtained from Merck. Furthermore, [6,6]-phenyl-C_{61}-butyric acid methyl ester (PCBM, 99.9%) and Bathocuproine (BCP, 99.99%) were sourced from Sigma-Aldrich (Tokyo, Japan). Silver wire (Ag, 99.999% purity) was procured from Nilaco Corp. (Tokyo, Japan). Electron acceptors used were either previously published [26] or the complete synthetic details can be found in the Supporting Information.

2.2. Device Fabrication

The NiO_x thin film was made by dissolving 29.08 mg of $Ni(NO_3)_2.5H_2O$ in the 1000 µL ethanol 99.99% with constant stirring for 1000 rpm. Then, followed by filtering with PTFE 0.45 µ to filter some insoluble particles. The NiO_x thin film, serving as the hole transport layer, was deposited onto FTO-coated glass. The substrate was thoroughly cleaned using deionized water, acetone, and isopropyl alcohol, each undergoing 15 minutes of sonication. Afterward, it was dried with a nitrogen jet and subjected to plasma cleaning in an ozone atmosphere for 20 minutes. Subsequently, 100 µL of NiO_x precursor solution was dropped onto the substrate and evenly distributed using a spin-coater at 4000 rpm for 30 seconds, followed by annealing at 350 °C for 3 hours. The inverted perovskite solar cells were fabricated by depositing a precursor solution containing 1M PbI_2 and 1M MAI dissolved in 700 µL DMF and 300 µL DMSO, which had been stirred at 60°C for 12 hours. This solution was spin-coated onto a NiO_x thin film (acting as the hole transport layer) at 6000 rpm for 45 seconds, followed by annealing at 100°C for 15 minutes. Before deposition, the NiO_x layer underwent plasma cleaning in an ozone atmosphere for 10 minutes. Next, 20 mg/mL FFI or DPP compounds in chlorobenzene were deposited on perovskite using a spin-coater at 2000 rpm for 30 seconds and continued by drying at 105 °C. Moreover, PCBM in chlorobenzene and 0.5 mg/mL BCP in ethanol were

sequentially deposited via spin-coating at 1500 rpm for 30 seconds and 4000 rpm for 30 seconds, respectively. Finally, a 100 nm silver (Ag) electrode was deposited through vacuum evaporation under a vacuum pressure of 4.5×10^{-4} Pa. The final device configuration was: glass/FTO/NiO_x/$MAPbI_3$/molecular glass electron-acceptor compounds/PCBM/BCP/Ag.

3. Results and discussion

Various small-molecule electron-acceptor derivatives can improve the performance of perovskite-based solar cells. Small-molecule electron acceptors are promising because they have multiple conjugated and delocalized double bonds, making them suitable as electron transport layers (ETLs) in perovskite solar cells (PSCs). The materials developed by our group are even more unique due to their glass-forming properties, which allow them to be deposited from solution as amorphous thin films. In this study, two new glass-forming fused fluoranthene imide (FFI) derivatives **1** and **2**, along with previously reported as diketopyrrolopyrrole (DPP) derivative **3** (3,3'-Bis(6-hexyl-1,3-dihydro-2H-indol-2-one)-2,2'-bithiophene-5,5'-dicarboxamide) [26] were studied. The structure of those materials is shown in **Figure 1**.

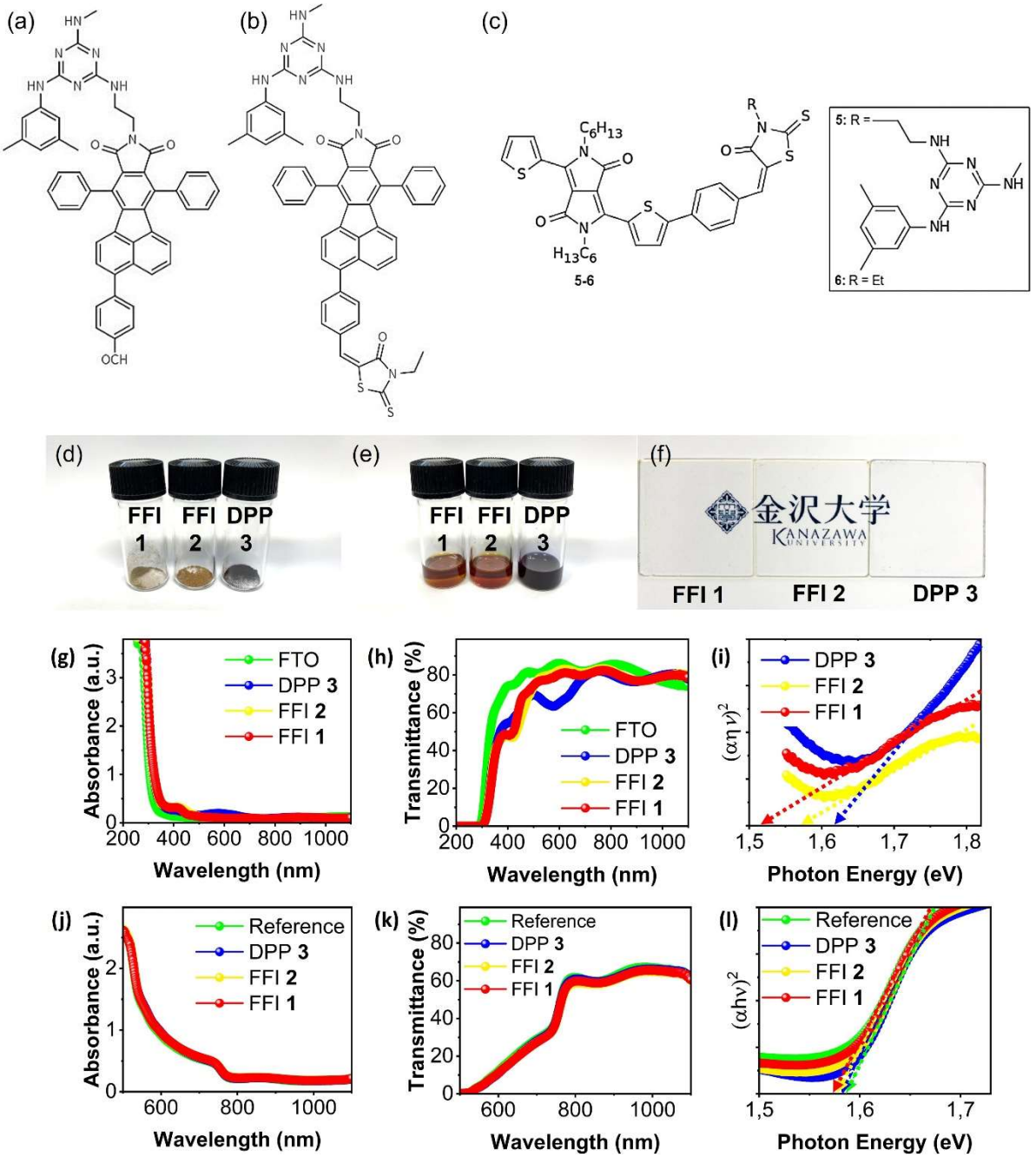

Figure 1. The structure of (a) FFI **1**, (b) FFI **2**, and (c) DPP **3**, and appearance of the compounds (d) before, (e) after dissolved in chlorobenzene, and its appearance (f) after deposited on glass. The optical properties of FFI **1**, FFI **2**, and DPP **3** for its (g) absorbance, (h) transmittance, (i) Tauc plot respectively. The optical properties of perovskite with FFI **1**, FFI **2**, and DPP **3** for its (j) absorbance, (k) transmittance, and (l) Tauc plot.

There are three ways that can be envisaged to introduce a mexylaminotriazine moiety on the FFI core: 1) on the imide side chain, 2) on one on the phenyl rings, or 3) on the fused naphthalene ring. Functionalizing the imide with the glass-inducing group enables a simple and divergent approach to screening different structures, even though it may not be optimal from a

purely cost perspective. For this purpose, previously published amino glass **4** was converted to the corresponding maleimide **5** in 55% yield by condensation of the free -NH_2 group with maleic anhydride. This reaction was a half pathway to synthesis FFI **1** and FFI **2**. The reaction pathway is shown in **Figure 2**.

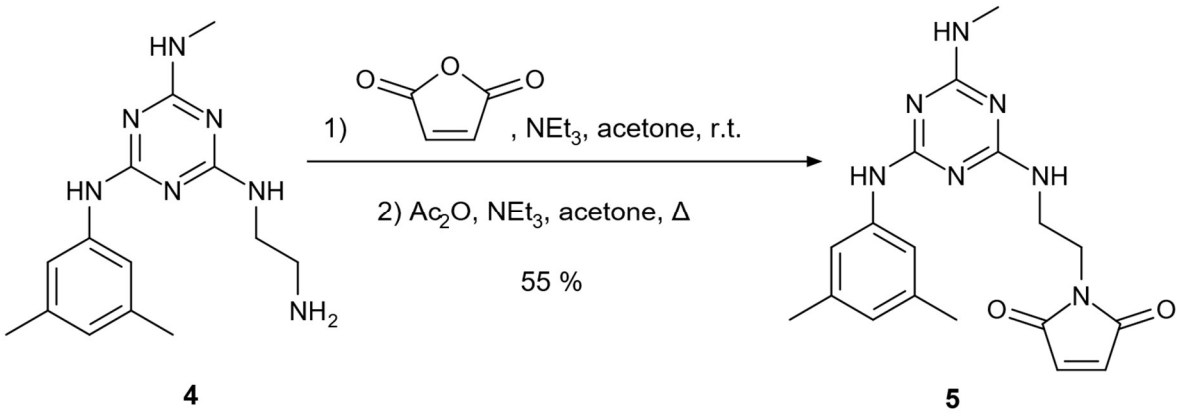

4 **5**

Figure 2. Synthesis reaction of maleimide compound from amino glass compound.

Moreover, maleimide glass **5** was then condensed via a cycloaddition reaction with cyclopentadienone **6** in refluxing nitrobenzene to afford mexylaminotriazine-substituted FFI glass **7** in 33% yield. Glass **7** is substituted with a bromo group on its naphthalene ring system, enabling further substitution with electron-withdrawing substituents to enhance its electron acceptor character. A 4-formylphenyl group was introduced via Suzuki coupling to yield aldehyde 5, which was then condensed with N-ethylrhodanine to afford rhodanine-substituted FFI **6**, in 67 and 95% yields, respectively. Compounds **4** and **5** could be conveniently purified by simple filtration on a short silica pad, while FFI **6** could be purified by reprecipitation. The successful synthesis of the intermediate and final glass-forming compounds was confirmed by ^{1}H, ^{13}C, and HSQC NMR spectroscopy, displaying the expected chemical shifts and correlations for all major protons and carbons as listed in **Figures S2–S13**. The complete synthesis reaction of FFI **1** and FFI **2** is shown in **Figure 3**.

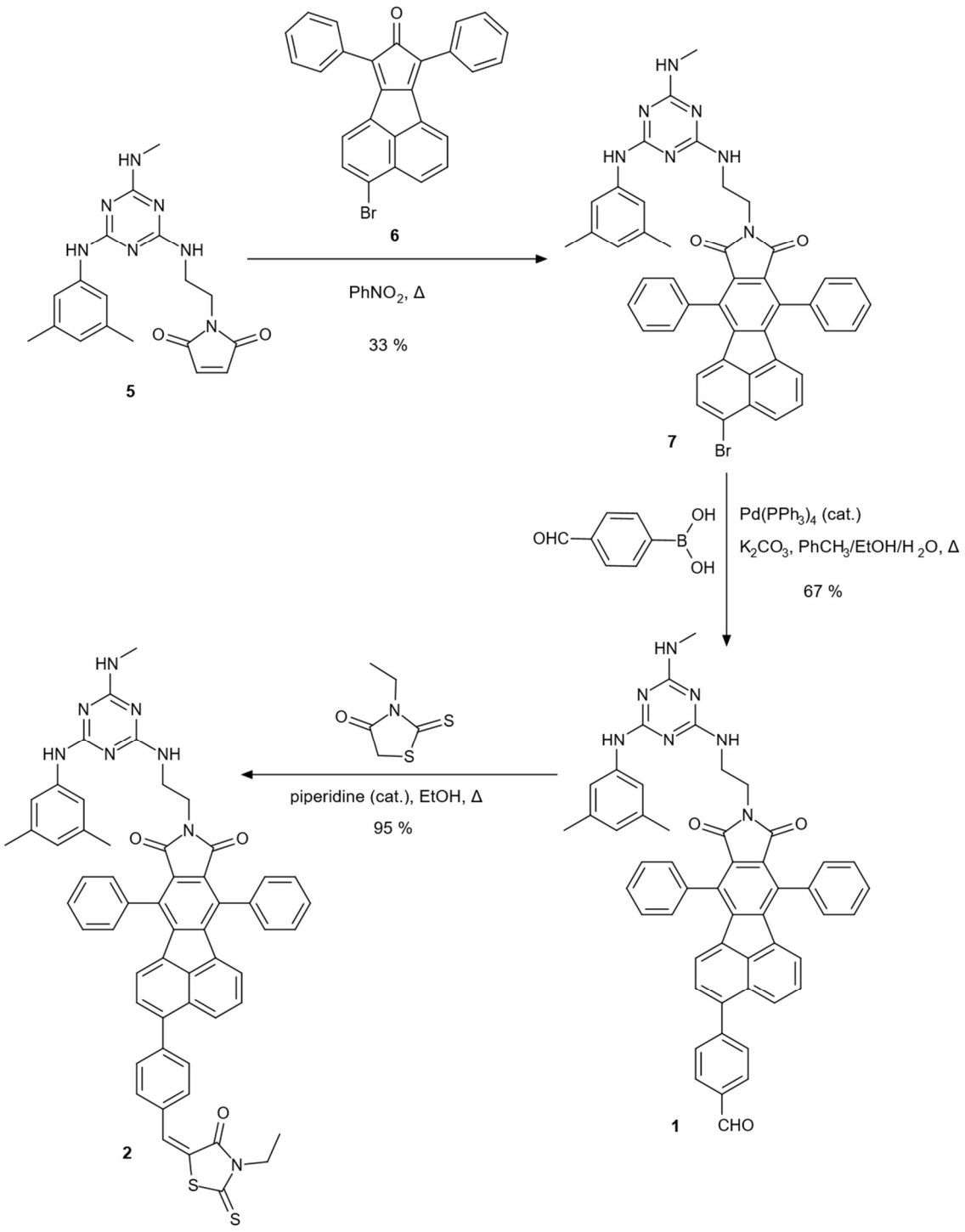

Figure 3. Complete synthesis pathway of FFI **1** (shown as structure number 1) and FFI **2** (shown as structure number 2) from maleimide compound.

As with most mexylaminotriazine-substituted derivatives, precursor **5** expectedly showed glass formation with no recrystallization on heating or slow cooling, with a glass transition temperature (T_g) of 72 °C, which is in the expected range for similar compounds. This glass-forming ability was successfully introduced in FFI derivatives **1**-**2** and **7**, which all showed T_g

values ranging from 147-173 °C, which are to be expected given the highly fused aromatic structures of the FFI moiety and the absence of long flexible chains. Again, no crystallization was observed for any of FFI glasses **1**-**2** and **7** under any conditions.

These materials serve as electron donor components in bulk heterojunction (BHJ) PSCs, where they are blended with electron acceptors, such as PCBM or Y6-based acceptors, to enhance charge separation and transport. The optical properties of the three electron-acceptors studied are crucial to their application in perovskite solar cells, making characterizations such as absorbance, transmittance, and band gap essential. In order to determine the optical properties of each electron acceptor, measurements were conducted by UV-Vis spectrophotometry. The UV-Vis absorption spectra of molecular glass electron-acceptor compounds provide crucial insights into their electronic properties and photovoltaic potential. The measured optical band gaps of 1.63 eV for DPP **3**, 1.57 eV for FFI **1**, and 1.59 eV for FFI **2** indicate their ability to absorb light in the visible to near-infrared (NIR) range, all compounds exhibit low absorption at wavelengths above 370 nm, making them promising donor materials in perovskite solar cells. Moreover, these band gaps correlate with the energy required for electron excitation from the Highest Occupied Molecular Orbital (HOMO) to the Lowest Unoccupied Molecular Orbital (LUMO), which directly influences charge transport efficiency. The HOMO and LUMO levels of each material were estimated based on their optical band gaps. The spectra of FFI **1** and FFI **2** display similar transmittance patterns, which can be attributed to their structural similarity. And due to their favourable band alignment, FFI **1** and FFI **2**, show the high potential for maximizing light absorption and improving photocurrent generation. DPP **3** exhibits a distinct transmittance pattern due to its fundamentally different structure. In addition, the boundary molecular orbitals of FFI 1 and FFI 2, calculated by DFT, further confirm the electron-withdrawing nature of the triazine moiety and its efficient delocalization across the π-conjugated backbone, as shown in **Figure S1**. Furthermore, their tuneable energy levels make them promising candidates for ETLs in perovskite solar cells, where optimized charge extraction is crucial for high-performance devices. The optical properties of molecular glass electron-acceptor compounds are shown in **Figure 1**.

The UV-Vis spectrum data after depositing the molecular glass electron-acceptor compounds (FFI **1**, FFI **2**, and DPP **3**) on the perovskite layer reveal that the optical band gap remains within the range of 1.57 - 1.58 eV, closely matching the reference perovskite layer. This stability in the band gap suggests that the molecular glass electron-acceptor compounds do not significantly disrupt the perovskite's electronic structure. The absorption spectra of the molecular glass electron-acceptor compounds-modified perovskite layers closely follow the

reference perovskite curve, indicating minimal alteration in optical properties and suggesting that these materials do not strongly absorb in the measured range. However, slight shifts or broadening at the absorption edge hint at potential interfacial interactions, such as charge transfer or dipole effects, which could influence carrier dynamics. The presence of these materials at the interface may modify charge transport and extraction without drastically affecting the intrinsic optical properties of the perovskite layer. These observations suggest that molecular glass electron-acceptor compounds could serve as functional interlayers in perovskite solar cells, optimizing charge transport while maintaining the fundamental absorption characteristics of the perovskite. The optical properties of perovskite modified by molecular glass electron-acceptor compounds are shown in **Figure 1**.

Furthermore, thermal stability test conducted over 96 hours at 85 ºC simultaneously provides crucial insights into the effectiveness of molecular glass electron-acceptor compounds in enhancing the stability of perovskite materials. As observed in **Figure 4**, the perovskite films incorporated with molecular glass electron-acceptor compounds exhibit remarkable stability, maintaining their structural integrity and visual uniformity throughout the test period. This suggests that molecular glass electron-acceptor compounds may act as protective layers, mitigating thermal degradation by preventing ion migration, inhibiting moisture penetration, or reducing defect formation at the interface. Typically, perovskite materials are prone to degradation under prolonged thermal stress, leading to phase segregation, oxidation, or decomposition. However, the preserved appearance of the molecular glass electron-acceptor modified films indicates that these materials enhance the perovskite's resistance to thermal-induced degradation, potentially extending the operational lifetime of perovskite solar cells. Further analysis, such as UV-Vis spectra and XRD, could confirm whether the structural and electronic properties remain intact, reinforcing the role of molecular glass electron-acceptor compounds in stabilizing perovskite materials under thermal stress. These findings highlight the potential of molecular glass electron-acceptor compounds-functionalized interfaces in improving the long-term performance and commercial viability of perovskite-based photovoltaic devices. **Figure 4** presents the UV-Vis spectra for the thermal stability of perovskite: (a) pristine perovskite as reference, perovskite with (b) FFI **1**, (c) FFI **2**, and (d) DPP **3**.

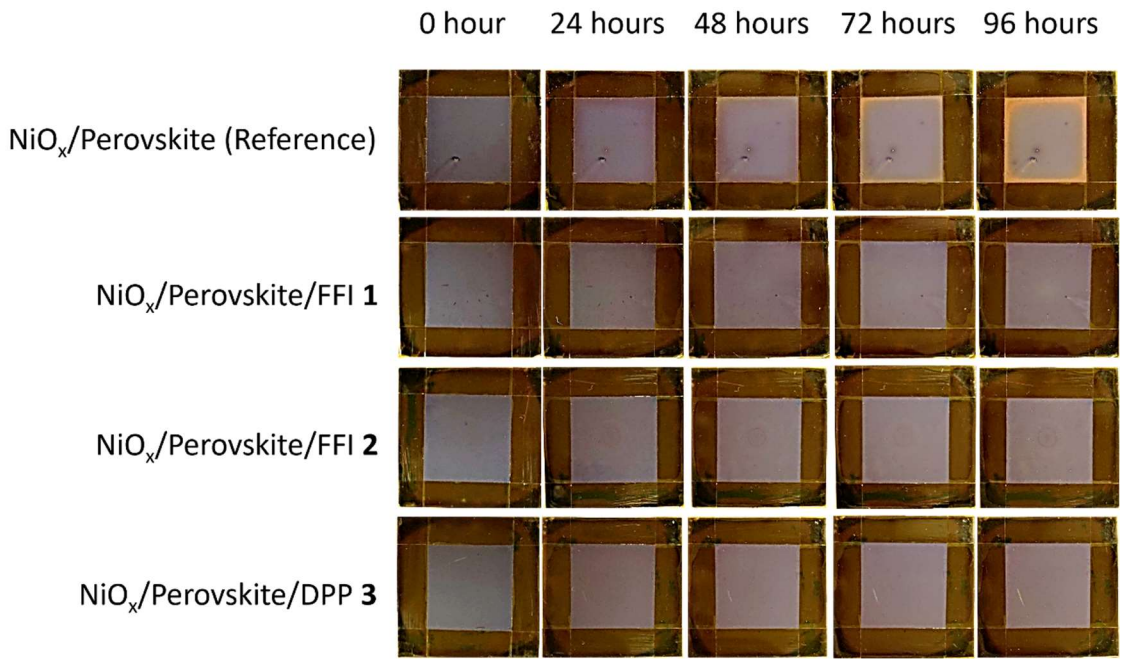

Figure 4. The appearance of perovskite with and without FFI **1**, **2**, and DPP **3** compounds on thermal stability test.

The complete set of UV-Vis spectra recorded during the 96-h thermal stability test is provided in the Supporting Information (**Figure S14**), which further confirms that the molecular glass-modified perovskite film retains its spectral profile and band edge positions, indicating suppressed thermal degradation compared to the pristine reference. The UV-Vis absorbance spectra shown in the image provide quantitative evidence supporting the thermal stability of perovskite materials incorporated with molecular glass electron-acceptor compounds over a 96-hour period at 85 °C. The absorbance curves at different time intervals (0 h, 24 h, 48 h, 72 h, and 96 h) show a gradual decrease in absorption intensity, a common characteristic of material degradation. However, the overall spectral shape and absorption edge remain relatively unchanged, indicating that the core optical properties of the perovskite layers are well preserved. Comparing these results with the thermal stability test images, it is evident that the molecular glass electron-acceptor compounds contribute to maintaining the structural and electronic integrity of the perovskite films. The minor reduction in absorbance suggests that some degradation occurs over time, likely due to thermal stress, but the perovskite films with molecular glass electron-acceptor compounds remain optically active and structurally intact. This aligns with the hypothesis that the molecular glass electron-acceptor compounds act as protective interlayers, reducing ion migration and preventing decomposition pathways that typically lead to perovskite degradation. Furthermore, the stability observed in the UV-Vis

spectra implies that the band gap energy of the perovskite remains nearly unchanged, ensuring that charge carrier generation and transport properties are not significantly compromised over the 96-hour test. This is crucial for the long-term performance of perovskite solar cells, as maintaining high absorption efficiency directly correlates with sustained photovoltaic performance. **Figure S14** shows the impact of molecular glass electron-acceptor compounds on the perovskite layer under thermal stability test.

Moreover, **Figure 5** shows the XRD pattern for the thermal stability of the perovskite with molecular glass electron-acceptor compounds. The XRD patterns of perovskite films measured over different aging times (0–96 h) are compared, with pristine perovskite (a) and perovskite films containing additives FFI **1** (b), FFI **2** (c), and DPP **3** (d). The main diffraction peaks are marked with symbols: δ corresponding to the δ-phase perovskite (undesired non-photoactive phase), α to the α-phase perovskite (desired photoactive black phase), and * representing PbI_2, which is typically a degradation by-product. In the pristine perovskite (a), the diffraction peaks indicate the coexistence of α-phase perovskite along with the gradual formation of PbI_2 and δ-phase over time. The intensity of the PbI_2 peak (12.62°) increases with longer storage, clearly showing the instability of the pristine perovskite and the decomposition pathway toward PbI_2. When the molecular glass electron-acceptor compounds were introduced (b, c, and d), the XRD patterns revealed a slower increase in the PbI_2 peak intensity compared to the pristine sample, indicating that FFI 1 helps suppress perovskite degradation. The α-phase peaks are maintained more strongly over 96 h, suggesting enhanced structural stability. The evidence of perovskite degradation is apparent in the XRD pattern in **Figure 5**, where the diffraction peak located at $2\theta = 14.00°$ corresponds to the (100) plane, which is the primary signature of the perovskite crystal structure and indicates good crystallinity of the α-phase halide perovskite. Meanwhile, the peak observed at $2\theta = 20.11°$ is assigned to the (110) plane of the perovskite lattice, representing a secondary but characteristic reflection of the perovskite structure[35–38].

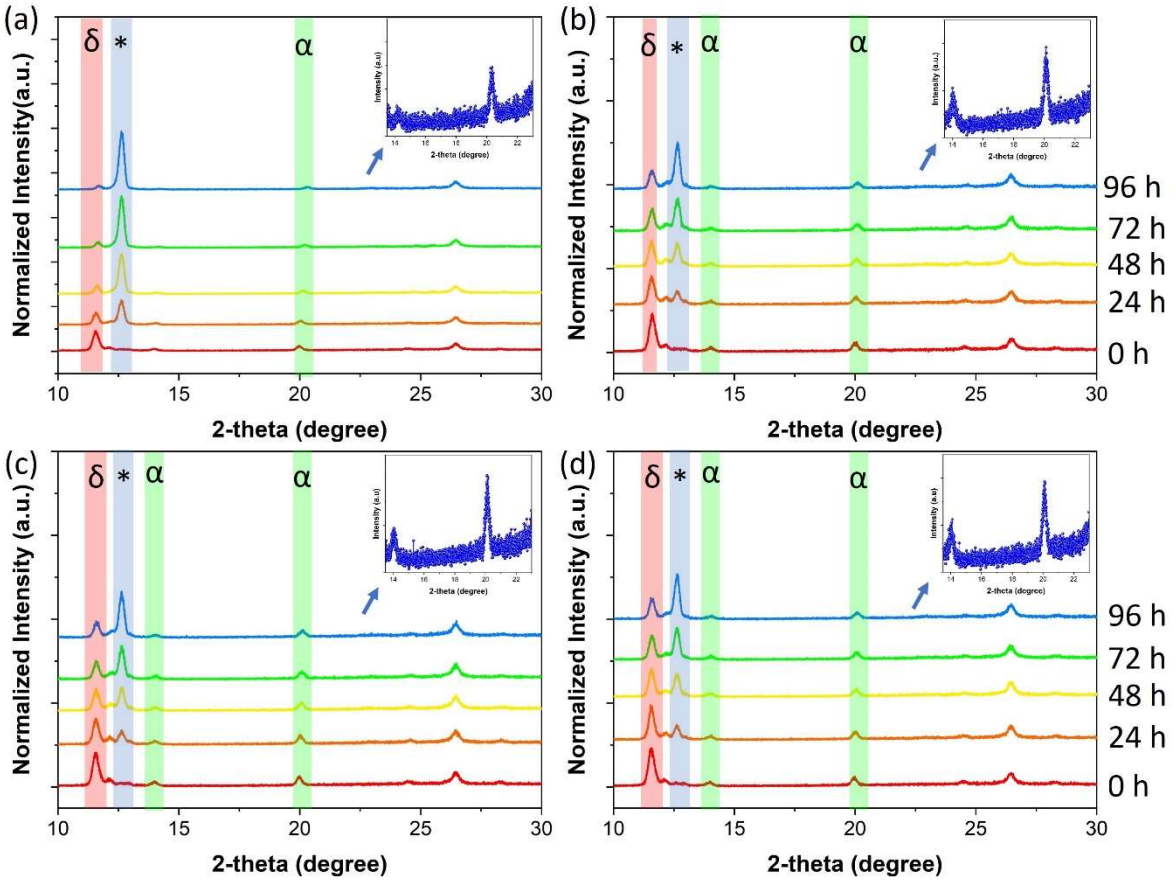

Figure 5. The XRD pattern of pristine perovskite on thermal stability as a (a) reference compared with perovskite added with (b) FFI **1**, (c) FFI **2**, and (d) DPP **3**.

The mechanism of perovskite decomposition has been extensively discussed by many researchers, with one of the main causes being the reaction between perovskite and water. Perovskite can also decompose into MAI and PbI_2. MAI can diffuse into the PCBM layer or evaporate as a gas, leaving behind yellow-coloured PbI_2 as a degradation residue. Therefore, the structural degradation of perovskite can also be visually identified by changes in its colour. If the perovskite layer begins to turn yellow, it indicates the formation of PbI_2, signalling the onset of decomposition. However, this phenomenon does not occur in perovskite layers that incorporate molecular glass electron-acceptor compounds. Molecular glass electron-acceptor compounds are well known for their extensive π-conjugated systems, which enable strong π-π interactions, resulting in enhanced electron delocalization and mobility. This feature is crucial for ETLs, as it enables efficient charge extraction from the perovskite layer to the electrode, minimizing charge recombination. The molecular glass electron-acceptor compounds have

highly planar structures, promoting tight molecular packing and superior charge transport properties compared to conventional organic ETLs like PCBM.

Moreover, when molecular glass electron-acceptor compounds are introduced, a perovskite-molecular glass electron-acceptor compounds interface layer forms, exhibiting hydrophobic properties. This hydrophobicity arises from the extensive conjugated and delocalized bonds within the molecular glass electron-acceptor compounds, which effectively repel atmospheric water molecules and hydrophilic MAI molecules. This hydrophobicity can be seen from the contact angle of molecular glass electron-acceptor compounds on the perovskite surface in **Figure 6**, which increased from 77° in pristine perovskite to 107.0°, 108.4°, and 108.3° for FFI **1**, FFI **2**, and DPP **3**, respectively. As a result, MAI does not diffuse into the PCBM layer or escape into the environment, leading to improved perovskite stability. The contact angles of water on molecular glass electron-acceptor compounds on perovskite are shown in **Figure 6**.

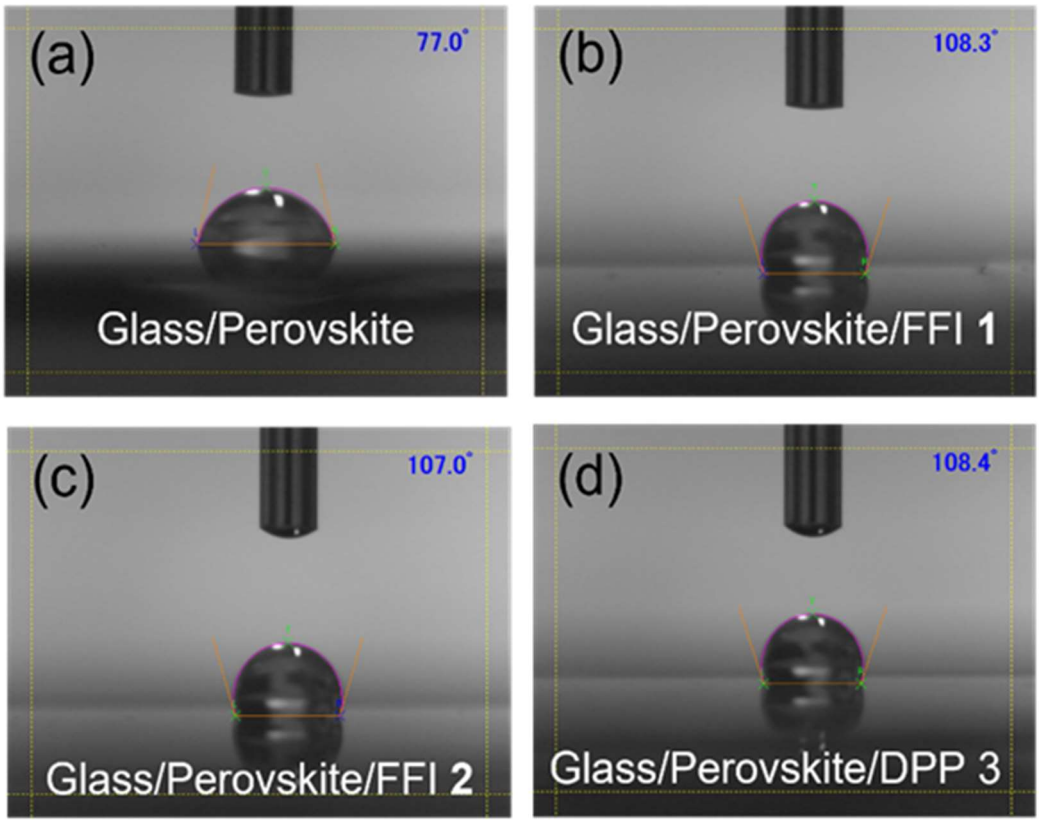

Figure 6. Contact angle test of perovskite with and without FFI **1**, FFI **2**, and DPP **3** compounds after 96 hours stability test.

Moreover, this hydrophobic perovskite-molecular glass electron-acceptor compounds interface enhances the compatibility between the perovskite and PCBM layers. This is because molecular glass electron-acceptor compounds share structural similarities with PCBM, including delocalized conjugated bonds and hydrophobicity, ensuring better interfacial contact. Additionally, molecular glass electron-acceptor compounds can still interact well with perovskite due to the triazine and thiophene functional groups, which can bind with the perovskite structure, further enhancing its stability. The decomposition and stability mechanisms are illustrated in **Figure 7**.

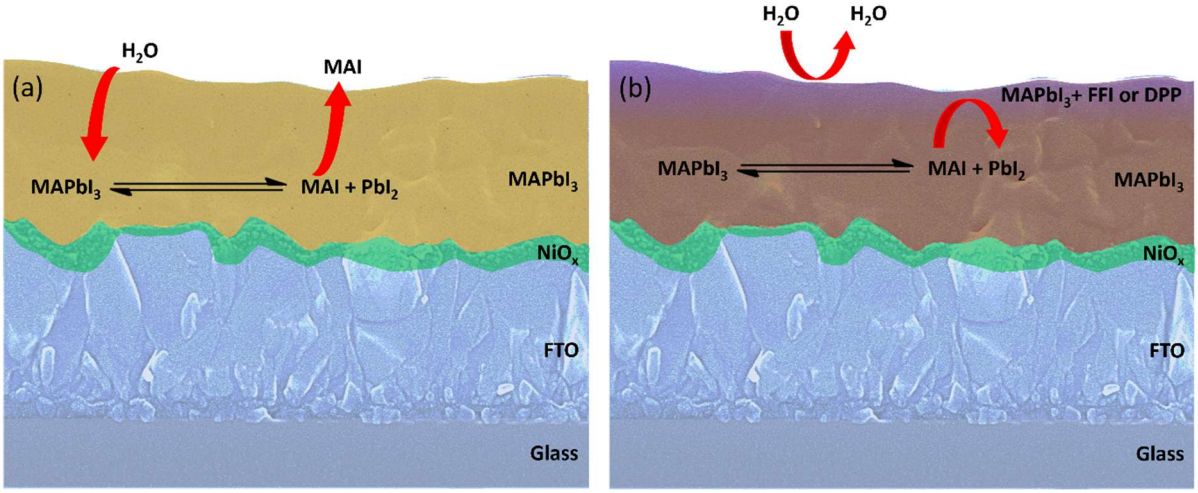

Figure 7. (a) The illustration of perovskite degradation on thermal stability test and (b) stability mechanism of perovskite due to added by molecular glass electron-acceptor compounds. The structure for thermal stability test was glass/FTO/NiO_x/$MAPbI_3$/molecular glass electron-acceptor compounds.

The hydrophobicity of molecular glass electron-acceptor compounds, resulting from conjugated and delocalized double bonds, enables them to repel external water molecules from the perovskite. This effectively suppresses perovskite degradation into MAI and PbI_2 while preventing MAI from reacting with PCBM and blocking PCBM diffusion into perovskite grain boundaries. Additionally, the molecular glass electron-acceptor compounds interlayer facilitates smooth electron migration from perovskite to PCBM, minimizing ion migration. These combined effects significantly enhance the long-term thermal stability of the perovskite film when molecular glass electron-acceptor compounds are used as ETLs.

Furthermore, SEM images confirm that molecular glass electron-acceptor compounds effectively coat the perovskite surface and penetrate its grain boundaries, forming a protective hydrophobic layer. This encapsulation effect prevents moisture infiltration and thermal-

induced degradation, thus improving the perovskite's resilience to environmental stressors. Consequently, the presence of molecular glass electron-acceptor compounds contributes to enhanced hydrophobicity and thermal stability, making this approach promising. **Figure 8** shows the SEM image of pristine perovskite as a reference and perovskite added with molecular glass electron-acceptor compounds.

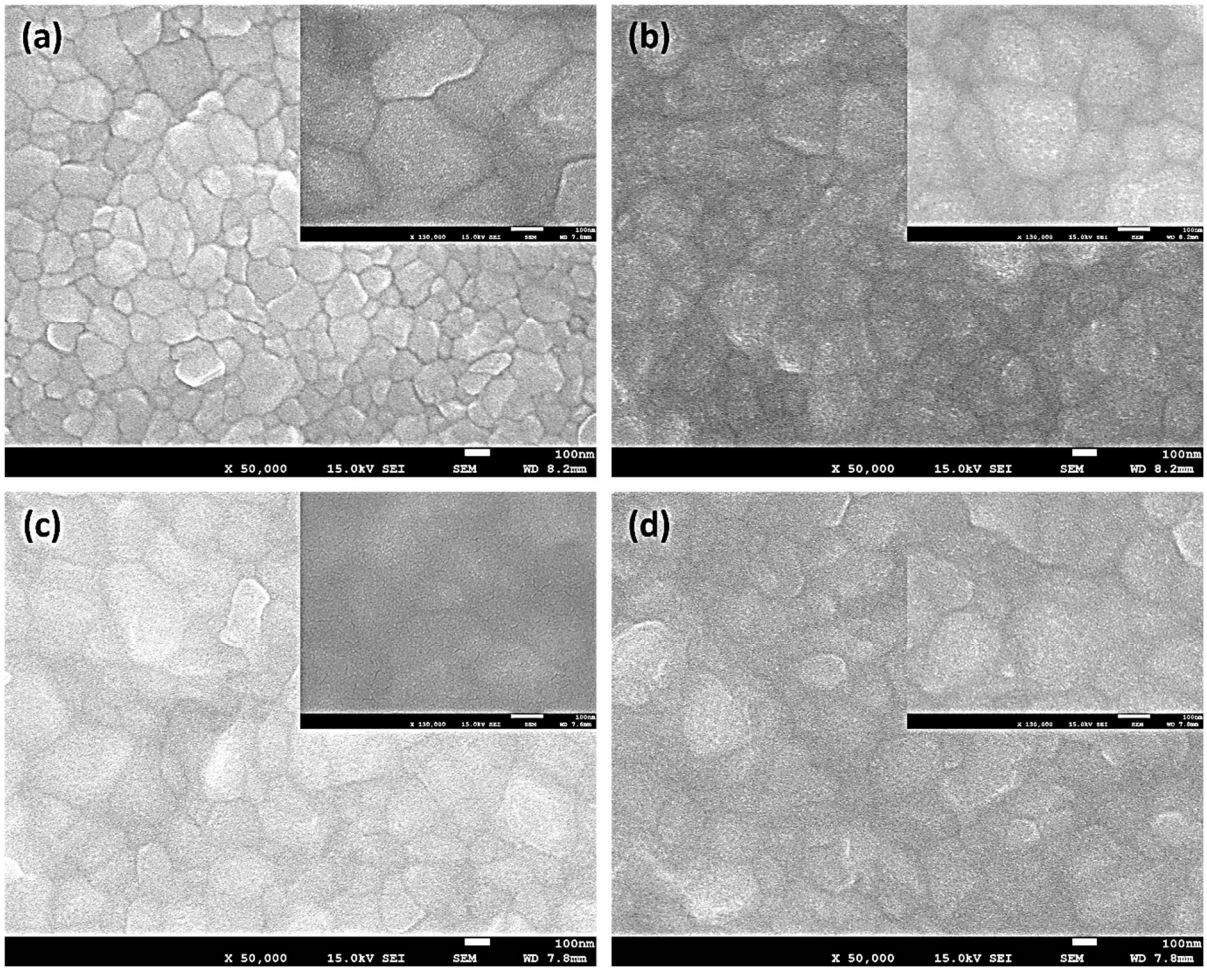

Figure 8. SEM image of (a) pristine perovskite as a reference, perovskite with (b) FFI **1**, (c) FFI **2**, and (d) DPP **3**.

Figure 9a presents the reverse scan *J–V* characteristics of perovskite solar cells fabricated without additives and with molecular glass electron-acceptor compounds. The plots clearly demonstrate variations in *Jsc* and *Voc* depending on the incorporated molecular glass. The reference device yields a *Jsc* of 17.86 mA/cm² and a *Voc* of 1.06 V, values typical of pristine perovskite solar cells. Upon the addition of molecular glass, the *J–V* behaviour is distinctly modified. Among all samples, the device with FFI **1** achieves the highest *Jsc*, suggesting more efficient charge generation and extraction. This improvement can be attributed to enhanced

film quality, higher crystallinity, and suppression of trap-assisted recombination. FFI **2** and DPP **3** also produce stable *J–V* curves with comparable *Voc* to the reference, although their *Jsc* values remain slightly lower than that of FFI **1**. In particular, the performance of DPP **3** is close to the reference, reflecting modest gains in current density but improved device stabilization. These findings confirm that molecular glass additives enhance overall photovoltaic performance, with FFI **1** providing the most pronounced effect.

The *J–V* data further reveal improvements across all key photovoltaic parameter (PCE, *Jsc*, *Voc*, and FF) when molecular glass-based interlayers are introduced. Notably, FFI **2** records the highest *Jsc* of 18.50 mA/cm², demonstrating superior charge collection. Meanwhile, *Voc* increases slightly to 1.08 V for both FFI **1** and FFI **2**, indicating better energy-level alignment between the perovskite absorber and ETL. The fill factor remains stable across devices, showing that the additives do not introduce significant series resistance or additional recombination losses. The reduced hysteresis between forward and reverse scans further suggests the suppression of ion migration and improved interfacial charge transport. These effects are corroborated in **Figure S15**, which compares *J–V* curves at maximum PCE for devices with and without molecular glass.

The molecular design of these additives plays a crucial role in enhancing performance. Triazine moieties provide strong electron-withdrawing properties, resulting in favourable energy-level alignment with the perovskite conduction band and facilitating efficient electron injection. Thiophene units, on the other hand, contribute molecular flexibility and improved charge transfer, which enhance overall transport characteristics[39,40]. As a result, the modified devices achieve higher PCEs than the reference: FFI **1** reaches 15.49% (reverse scan), followed by FFI **2** at 15.20% and DPP **3** at 14.94%. These improvements demonstrate the ability of molecular glass electron-acceptor compounds to enhance charge extraction and mitigate recombination losses, as illustrated in **Figure 9b**.

Further insights are obtained from the dark *I–V* characteristics. Molecular glass-based devices exhibit significantly reduced leakage currents compared to the reference, confirming better charge-blocking capability and suppression of recombination at the interfaces. The presence of triazine and thiophene groups within the interlayer enhances charge mobility and energy-level alignment, facilitating efficient electron transfer from the perovskite to PCBM. Lower dark current indicates effective suppression of ion migration and reduced charge accumulation, both of which contribute to improved interfacial stability and longer operational lifetimes. As shown in **Figure 9c**.

The stability benefits of molecular glass incorporation are also evident. the modified devices maintain lower leakage currents, while maximum power point tracking consistently demonstrates higher and more stable power outputs. The sustained performance of FFI **1**, FFI **2**, and DPP **3** under continuous illumination underscores their role in minimizing ion migration, charge accumulation, and perovskite degradation as shown in **Figure 9d**. Altogether, these results confirm that molecular glass electron-acceptor compounds not only enhance efficiency but also provide long-term operational stability in perovskite solar cells.

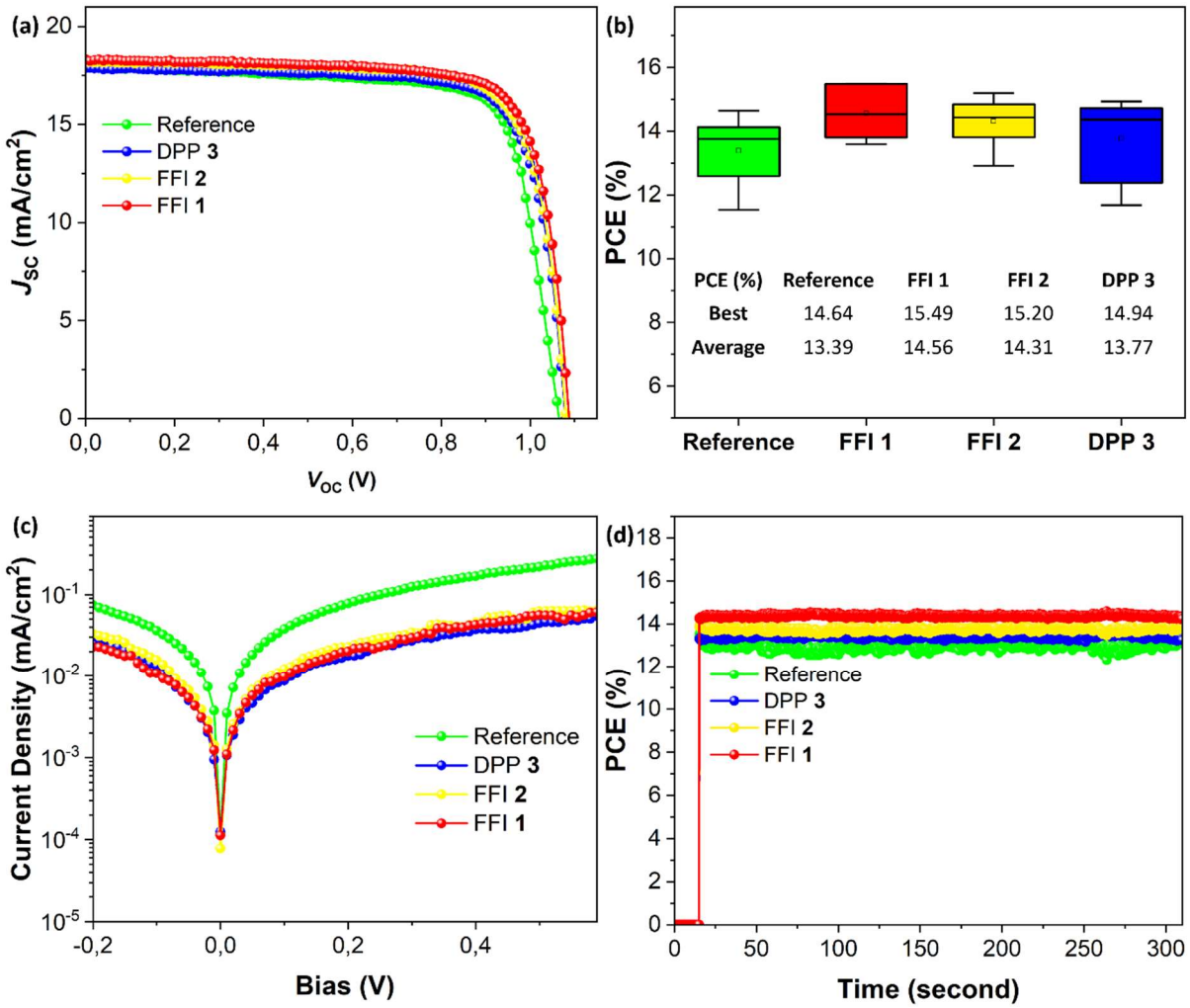

Figure 9. (a) The reverse scan *J–V* characteristics of perovskite solar cells fabricated without additives and with molecular glass additives FFI **1**, FFI **2**, and DPP **3**, (b) PCE comparison of pristine perovskite as reference, FFI **1**, FFI **2**, and DPP **3**, (c) comparison of dark *I-V* curve with and without molecular glass electron-acceptor compounds and (d) comparison MPPT curve perovskite with and without molecular glass electron-acceptor compounds.

Moreover, the data clearly indicate the significant enhancement in device performance when molecular glass electron-acceptor compounds are introduced as an interfacial layer

between perovskite and PCBM. The reference device, which employs only PCBM as the ETL, exhibits a moderate PCE, with relatively lower *Jsc* and *Voc*, likely due to suboptimal charge extraction and increased recombination at the interface. In contrast, PSCs modified with molecular glass electron-acceptor compounds show a substantial improvement in all key photovoltaic parameters. This improvement is attributed to the strong π-π stacking interactions in the molecular glass electron-acceptor compounds, which enhance charge transport, and the presence of triazine and thiophene functionalities, which facilitate better energy level alignment and suppress interfacial defects. Among the FFI **1**, FFI **2**, and DPP **3**-based interlayers, FFI **2** demonstrates the highest PCE, indicating its superior ability to improve charge extraction and stability. The higher *Jsc* observed in FFI **2**-modified devices suggests more efficient electron collection, while the increase in *Voc* implies reduced non-radiative recombination losses. Moreover, the FF is significantly improved, signifying reduced series resistance and enhanced charge transfer dynamics. The DPP **3** and FFI **1** interlayers also exhibit improved performance compared to the reference, though slightly lower than FFI **2**, reinforcing the beneficial effects of FFI **1**, FFI **2**, and DPP **3** compounds. **Table 1** provides a detailed comparison of the photovoltaic parameters such as PCE, *Jsc*, *Voc*, and FF for the reference device and perovskite solar cells integrated with various molecular glass compound interlayers.

Table 1. Comparison of *J-V* curve with and without molecular glass electron-acceptor compounds at best PCE

Device	Scan direction	J_{SC} (mA/cm^2)	V_{OC} (V)	FF	PCE (%)
Reference	Forward	17.54	1.06	0.75	14.01
	Reverse	17.95	1.06	0.77	14.64
FFI 1	Forward	18.44	1.08	0.76	15.17
	Reverse	18.32	1.08	0.78	15.49
FFI 2	Forward	18.50	1.07	0.76	15.06
	Reverse	18.20	1.08	0.77	15.20
DPP 3	Forward	18.05	1.07	0.76	14.61
	Reverse	17.87	1.07	0.78	14.94

Conclusions

This work demonstrates that glass-forming molecular electron-acceptor compounds serve as highly effective interfacial layers for inverted $MAPbI_3$ perovskite solar cells. By

adding FFI **1**, FFI **2**, and DPP **3** between the perovskite absorber and PCBM, we observed a significant improvement in photovoltaic performance, with power conversion efficiencies (PCEs) increasing from 14.6% (reference) to 15.5% (FFI 1), 15.2% (FFI 2), and 14.9% (DPP 3). Water contact angles increased from 77° to over 108°, indicating the formation of durable hydrophobic barriers that hinder MAI diffusion and PbI_2 formation. Under continuous maximum power point tracking at 85 °C, FFI-modified cells maintained over 90% of their initial PCE after 96 hours, while unmodified cells degraded within 48 hours. Mechanistic studies highlight the benefits of strong π–π stacking, electron-withdrawing triazine/thiophene groups, and amorphous glass-like morphology. X-ray diffraction and UV–Vis analysis show the preservation of α-phase structure with minimal PbI_2 growth, while dark I–V and hysteresis tests confirm reduced leakage currents and suppressed ion migration. SEM and contact-angle measurements reveal uniform interlayer coverage and improved interfacial compatibility with PCBM, leading to better charge extraction and stability over time.

Looking ahead, these findings suggest several pathways for advancing molecular glass interfacial engineering in next-generation perovskite photovoltaics:

- Expand stability testing to include combined humidity and light exposure to better predict real-world operational lifetimes.

- Design molecular glass derivatives with varied side chains or core structures to optimize energy-level alignment and processability.

- Incorporate interlayers into mixed-cation/halide perovskites and tandem cell configurations to achieve efficiencies exceeding 20%.

- Develop scalable deposition techniques, such as slot-die coating or roll-to-roll printing, for large-area modules.

- Combine molecular glass interlayers with advanced hole-transport materials and encapsulation strategies to meet IEC and IEC standards.

Acknowledgements:

This study was partially supported by a Grant-in-Aid for Scientific Research (Grant Number 24K17769). Research at Queens was also supported by the the Natural Sciences and Engineering Research Council of Canada (RGPIN-2020-07016). The authors also extend their

appreciation to the research support by the Deanship of Graduate Studies and Scientific Research at the Islamic University of Madinah, Saudi Arabia.

References

(1) Zhou, J.; Tan, L.; Liu, Y.; Li, H.; Liu, X.; Li, M.; Wang, S.; Zhang, Y.; Jiang, C.; Hua, R.; Tress, W.; Meloni, S.; Yi, C. Highly Efficient and Stable Perovskite Solar Cells via a Multifunctional Hole Transporting Material. *Joule* 2024, *8* (6), 1691–1706. https://doi.org/10.1016/J.JOULE.2024.02.019.

(2) Chen, H.; Liu, C.; Xu, J.; Maxwell, A.; Zhou, W.; Yang, Y.; Zhou, Q.; Bati, A. S. R.; Wan, H.; Wang, Z.; Zeng, L.; Wang, J.; Serles, P.; Liu, Y.; Teale, S.; Liu, Y.; Saidaminov, M. I.; Li, M.; Rolston, N.; Hoogland, S.; Filleter, T.; Kanatzidis, M. G.; Chen, B.; Ning, Z.; Sargent, E. H. Improved Charge Extraction in Inverted Perovskite Solar Cells with Dual-Site-Binding Ligands. *Science (1979)* 2024, *384* (6692), 189–193. https://doi.org/10.1126/SCIENCE.ADM9474/SUPPL_FILE/SCIENCE.ADM9474_SM.PDF.

(3) Azmi, R.; Utomo, D. S.; Vishal, B.; Zhumagali, S.; Dally, P.; Risqi, A. M.; Prasetio, A.; Ugur, E.; Cao, F.; Imran, I. F.; Said, A. A.; Pininti, A. R.; Subbiah, A. S.; Aydin, E.; Xiao, C.; Seok, S. Il; De Wolf, S. Double-Side 2D/3D Heterojunctions for Inverted Perovskite Solar Cells. *Nature* 2024, *628* (8006), 93–98. https://doi.org/10.1038/s41586-024-07189-3.

(4) Azmi, R.; Ugur, E.; Seitkhan, A.; Aljamaan, F.; Subbiah, A. S.; Liu, J.; Harrison, G. T.; Nugraha, M. I.; Eswaran, M. K.; Babics, M.; Chen, Y.; Xu, F.; Allen, T. G.; Rehman, A. ur; Wang, C.-L.; Anthopoulos, T. D.; Schwingenschlögl, U.; De Bastiani, M.; Aydin, E.; De Wolf, S. Damp Heat–Stable Perovskite Solar Cells with Tailored-Dimensionality 2D/3D Heterojunctions. *Science (1979)* 2022, *376* (6588), 73–77. https://doi.org/10.1126/science.abm5784.

(5) Liu, X.; Zheng, B.; Shi, L.; Zhou, S.; Xu, J.; Liu, Z.; Yun, J. S.; Choi, E.; Zhang, M.; Lv, Y.; Zhang, W.-H.; Huang, J.; Li, C.; Sun, K.; Seidel, J.; He, M.; Peng, J.; Hao, X.; Green, M. Perovskite Solar Cells Based on Spiro-OMeTAD Stabilized with an Alkylthiol Additive. *Nat Photonics* 2023, *17* (1), 96–105. https://doi.org/10.1038/s41566-022-01111-x.

(6) Gong, S.; Qu, G.; Qiao, Y.; Wen, Y.; Huang, Y.; Cai, S.; Zhang, L.; Jiang, K.; Liu, S.; Lin, M.; Beard, M. C.; Xu, Z.-X.; Chen, X. A Hot Carrier Perovskite Solar Cell with Efficiency Exceeding 27% Enabled by Ultrafast Hot Hole Transfer with Phthalocyanine Derivatives. *Energy Environ Sci* 2024, *17* (14), 5080–5090. https://doi.org/10.1039/D4EE01839G.

(7) Garcia, V. J.; Pelicano, C. M.; Yanagi, H. Low Temperature-Processed ZnO Nanorods-TiO2 Nanoparticles Composite as Electron Transporting Layer for Perovskite Solar Cells. *Thin Solid Films* 2018, *662*, 70–75. https://doi.org/10.1016/J.TSF.2018.07.039.

(8) Qureshi, A. A.; Javed, H. M. A.; Javed, S.; Bashir, A.; Usman, M.; Akram, A.; Ahmad, M. I.; Ali, U.; Shahid, M.; Rizwan, M.; Raza, S. A. Incorporation of Zr-Doped TiO2 Nanoparticles in Electron Transport Layer for Efficient Planar Perovskite Solar Cells. *Surfaces and Interfaces* 2021, *25*, 101299. https://doi.org/10.1016/J.SURFIN.2021.101299.

(9) Ono, L. K.; Juarez-Perez, E. J.; Qi, Y. Progress on Perovskite Materials and Solar Cells with Mixed Cations and Halide Anions. *ACS Applied Materials and Interfaces*. American Chemical Society September 13, 2017, pp 30197–30246. https://doi.org/10.1021/acsami.7b06001.

(10) Chen, P.; Xiao, Y.; Li, S.; Jia, X.; Luo, D.; Zhang, W.; Snaith, H. J.; Gong, Q.; Zhu, R. The Promise and Challenges of Inverted Perovskite Solar Cells. *Chem Rev* 2024, *124* (19), 10623–10700. https://doi.org/10.1021/acs.chemrev.4c00073.

(11) Gantumur, M.; Shahiduzzaman, M.; Hossain, M. I.; Akhtaruzzaman, M.; Nakano, M.; Karakawa, M.; Nunzi, J. M.; Taima, T. Revolutionizing Light Capture: A Comprehensive Review of Back-Contact Perovskite Solar Cell Architectures. *Materials Today*. Elsevier B.V. 2025. https://doi.org/10.1016/j.mattod.2025.08.017.

(12) Zhong, Y.; Hufnagel, M.; Thelakkat, M.; Li, C.; Huettner, S. Role of PCBM in the Suppression of Hysteresis in Perovskite Solar Cells. *Adv Funct Mater* 2020, *30* (23). https://doi.org/10.1002/adfm.201908920.

(13) Zhang, F.; Shi, W.; Luo, J.; Pellet, N.; Yi, C.; Li, X.; Zhao, X.; Dennis, T. J. S.; Li, X.; Wang, S.; Xiao, Y.; Zakeeruddin, S. M.; Bi, D.; Grätzel, M. Isomer-Pure Bis-PCBM-Assisted Crystal Engineering of Perovskite Solar Cells Showing Excellent Efficiency and Stability. *Advanced Materials* 2017, *29* (17), 1606806. https://doi.org/10.1002/ADMA.201606806.

(14) Shao, Y.; Xiao, Z.; Bi, C.; Yuan, Y.; Huang, J. Origin and Elimination of Photocurrent Hysteresis by Fullerene Passivation in CH3NH3PbI3 Planar Heterojunction Solar Cells. *Nat Commun* 2014, *5*. https://doi.org/10.1038/ncomms6784.

(15) Bi, E.; Chen, H.; Xie, F.; Wu, Y.; Chen, W.; Su, Y.; Islam, A.; Grätzel, M.; Yang, X.; Han, L. Diffusion Engineering of Ions and Charge Carriers for Stable Efficient Perovskite Solar Cells. *Nat Commun* 2017, *8*. https://doi.org/10.1038/ncomms15330.

(16) Wojciechowski, K.; Stranks, S. D.; Abate, A.; Sadoughi, G.; Sadhanala, A.; Kopidakis, N.; Rumbles, G.; Li, C. Z.; Friend, R. H.; Jen, A. K. Y.; Snaith, H. J. Heterojunction Modification for Highly Efficient Organic-Inorganic Perovskite Solar Cells. *ACS Nano* 2014, *8* (12), 12701–12709. https://doi.org/10.1021/NN505723H/SUPPL_FILE/NN505723H_SI_001.PDF.

(17) Muslih, E. Y.; Shahiduzzaman, Md.; Akhtaruzzaman, Md.; Hossain, M. I.; Wang, L.; Alkhammash, H. I.; Alharthi, S. S.; Nakano, M.; Karakawa, M.; Aminuzzaman, M.; Tey, L.-H.; Sopian, K.; Nunzi, J.-M.; Taima, T. Reproducible Perovskite Solar Cells Using a Simple Solvent-Mediated Sol−gel Synthesized NiOx Hole Transport Layer. *Applied Physics Express* 2022, *15* (1), 015504. https://doi.org/10.35848/1882-0786/ac435d.

(18) Marques, M. J. M.; Lin, W.; Taima, T.; Umezu, S.; Shahiduzzaman, M. Unleashing the Potential of Industry Viable Roll-to-Roll Compatible Technologies for Perovskite Solar Cells: Challenges and Prospects. *Materials Today*. Elsevier B.V. September 1, 2024, pp 112–141. https://doi.org/10.1016/j.mattod.2024.06.013.

(19) Shen, L.; Song, P.; Jiang, K.; Zheng, L.; Qiu, J.; Li, F.; Huang, Y.; Yang, J.; Tian, C.; Jen, A. K. Y.; Xie, L.; Wei, Z. Ultrathin Polymer Membrane for Improved Hole Extraction and Ion Blocking in Perovskite Solar Cells. *Nature Communications* 2024, *15* (1). https://doi.org/10.1038/s41467-024-55329-0.

(20) Gong, C.; Li, H.; Wang, H.; Zhang, C.; Zhuang, Q.; Wang, A.; Xu, Z.; Cai, W.; Li, R.; Li, X.; Zang, Z. Silver Coordination-Induced n-Doping of PCBM for Stable and Efficient Inverted Perovskite Solar Cells. *Nat Commun* 2024, *15* (1). https://doi.org/10.1038/s41467-024-49395-7.

(21) Shen, Z.; Han, Q.; Luo, X.; Shen, Y.; Wang, Y.; Yuan, Y.; Zhang, Y.; Yang, Y.; Han, L. Efficient and Stable Perovskite Solar Cells with Regulated Depletion Region. *Nat Photonics* 2024, *18* (5), 450–457. https://doi.org/10.1038/s41566-024-01383-5.

(22) You, S.; Eickemeyer, F. T.; Gao, J.; Yum, J. H.; Zheng, X.; Ren, D.; Xia, M.; Guo, R.; Rong, Y.; Zakeeruddin, S. M.; Sivula, K.; Tang, J.; Shen, Z.; Li, X.; Grätzel, M. Bifunctional Hole-Shuttle Molecule for Improved Interfacial Energy Level Alignment and Defect Passivation in Perovskite Solar Cells. *Nat Energy* 2023, *8* (5), 515–525. https://doi.org/10.1038/s41560-023-01249-0.

(23) Shahiduzzaman, Md.; Muslih, E. Y.; Hasan, A. K. M.; Wang, L.; Fukaya, S.; Nakano, M.; Karakawa, M.; Takahashi, K.; Akhtaruzzaman, Md.; Nunzi, J.-M.; Taima, T. The Benefits of Ionic Liquids for the Fabrication of Efficient and Stable Perovskite Photovoltaics. *Chemical Engineering Journal* 2021, *411*, 128461. https://doi.org/https://doi.org/10.1016/j.cej.2021.128461.

(24) Kapil, G.; Bessho, T.; Maekawa, T.; Baranwal, A. K.; Zhang, Y.; Kamarudin, M. A.; Hirotani, D.; Shen, Q.; Segawa, H.; Hayase, S. Tin-Lead Perovskite Fabricated via Ethylenediamine Interlayer Guides to the Solar Cell Efficiency of 21.74%. *Adv Energy Mater* 2021, *11* (25), 2101069. https://doi.org/https://doi.org/10.1002/aenm.202101069.

(25) Ali, H.; Ahmed, I.; Robertson, K.; Lanterna, A. E. PDI-Functionalized Glass Beads: Efficient, Metal-Free Heterogeneous Photocatalysts Suitable for Flow Photochemistry. *Org Process Res Dev* 2024. https://doi.org/10.1021/acs.oprd.4c00256.

(26) Adhikari, T.; Ghoshouni Rahami, Z.; Nunzi, J. M.; Lebel, O. Synthesis, Characterization and Photovoltaic Performance of Novel Glass-Forming Perylenediimide Derivatives. *Org Electron* 2016, *34*, 146–156. https://doi.org/10.1016/j.orgel.2016.04.025.

(27) Brar, D. S.; Aponte, R.; Tunge, J. Photoredox-Catalyzed Decarboxylative Elimination via Halogen Atom Transfer. *J Org Chem* 2025, *90* (15), 5274–5280. https://doi.org/10.1021/acs.joc.5c00237.

(28) Bhattacharjee, R.; Jervis, H.; McCormack, M. E.; Petrukhina, M. A.; Kertesz, M. Structure and Bonding in π-Stacked Perylenes: The Impact of Charge on Pancake

Bonding. *J Am Chem Soc* 2024, *146* (15), 10465–10477. https://doi.org/10.1021/jacs.3c14065.

(29) Li, S.; Wang, X.; Fang, J.; Lin, D.; Huang, N.; Wang, D.; He, S.; Qiu, L. Interfacial Competing Interaction Eliminates Voids in the Buried Interface for Efficient and Stable Perovskite Solar Modules on Bare NiOX. *Chemical Engineering Journal* 2024, *490*, 151919. https://doi.org/https://doi.org/10.1016/j.cej.2024.151919.

(30) Zhai, M.; Guo, Z.; Yang, J.; Chen, C.; Xia, Z.; Xu, H.; Wu, T.; Wang, P.; Yamada, S.; Tamada, K.; Matsushima, T.; Cheng, M. Interface Regulation with D-A-D Type Small Molecule for Efficient and Durable Perovskite Solar Cells. *Journal of Energy Chemistry* 2025, *107*, 832–840. https://doi.org/https://doi.org/10.1016/j.jechem.2025.04.010.

(31) Sharma, A.; Singh, R.; Kini, G. P.; Hyeon Kim, J.; Parashar, M.; Kim, M.; Kumar, M.; Kim, J. S.; Lee, J.-J. Side-Chain Engineering of Diketopyrrolopyrrole-Based Hole-Transport Materials to Realize High-Efficiency Perovskite Solar Cells. *ACS Appl Mater Interfaces* 2021, *13* (6), 7405–7415. https://doi.org/10.1021/acsami.0c17583.

(32) Cheng, H.; Zhao, X.; Shen, Y.; Wang, M.; Wang, L.; Meier, H.; Cao, D. Diketopyrrolopyrrole Based D-π-A-π-D Type Small Organic Molecules as Hole Transporting Materials for Perovskite Solar Cells. *Journal of Energy Chemistry* 2018, *27* (4), 1175–1182. https://doi.org/https://doi.org/10.1016/j.jechem.2017.08.007.

(33) Kini, G. P.; Parashar, M.; Shukla, V. K.; Singh, R. Deciphering the Effect of Replacing Thiophene with Selenophene in Diketopyrrolopyrrole (DPP)-Based Low Cost Hole Transport Materials on the Performance of Perovskite Solar Cells. *Sustain Energy Fuels* 2021, *5* (23), 5994–6003. https://doi.org/10.1039/D1SE01211H.

(34) Adhikari, T.; Nunzi, J. M.; Lebel, O. Solid-State Showdown: Comparing the Photovoltaic Performance of Amorphous and Crystalline Small-Molecule Diketopyrrolopyrrole Acceptors. *Org Electron* 2017, *48*, 230–240. https://doi.org/10.1016/j.orgel.2017.06.008.

(35) Amratisha, K.; Tuchinda, W.; Ruankham, P.; Naikaew, A.; Pansa-Ngat, P.; Srathongsian, L.; Wattanathana, W.; Shin Thant, K. K.; Supruangnet, R.; Nakajima, H.; Sahasithiwat, S.; Kanjanaboos, P. Graded Multilayer Triple Cation Perovskites for High Speed and Detectivity Self-Powered Photodetector via Scalable Spray Coating Process. *Sci Rep* 2022, *12* (1). https://doi.org/10.1038/s41598-022-14774-x.

(36) Cimrová, V.; Guesmi, M.; Eom, S.; Kang, Y.; Výprachtický, D. Formamidinium Lead Iodide Perovskite Thin Films Formed by Two-Step Sequential Method: Solvent–Morphology Relationship. *Materials* 2023, *16* (3). https://doi.org/10.3390/ma16031049.

(37) Ma, F.; Li, J.; Li, W.; Lin, N.; Wang, L.; Qiao, J. Stable α/δ Phase Junction of Formamidinium Lead Iodide Perovskites for Enhanced near-Infrared Emission. *Chem Sci* 2016, *8* (1), 800–805. https://doi.org/10.1039/c6sc03542f.

(38) Zhu, T.; Gong, X. Low-Dimensional Perovskite Materials and Their Optoelectronics. *InfoMat*. Blackwell Publishing Ltd October 1, 2021, pp 1039–1069. https://doi.org/10.1002/inf2.12211.

(39) Solis, O. E.; Mínguez-Avellán, M.; Betancur, P. F.; Sánchez- Alarcón, R. I.; Rodriguez, I.; Martínez-Pastor, J. P.; Ripolles, T. S.; Abargues, R.; Boix, P. P. Adjusting the Crystallization of Tin Perovskites through Thiophene Additives for Improved Photovoltaic Stability. *ACS Energy Lett* 2024, 5288–5295. https://doi.org/10.1021/acsenergylett.4c01875.

(40) Kim, J.; Yun, A. J.; Gil, B.; Lee, Y.; Park, B. Triamine-Based Aromatic Cation as a Novel Stabilizer for Efficient Perovskite Solar Cells. *Adv Funct Mater* 2019, *29* (44). https://doi.org/10.1002/adfm.201905190.